The Ollie: A Case Study in Trajectory Optimization with Varied Contacts

Nicholas Anderson[1], Stacey Shield[1] and Amir Patel[1]

***Abstract*—Modelling the discrete dynamics of contacts with objects and the environment is a challenging aspect of trajectory optimization. In this paper, we use the ollie, a skateboarding manoeuvre, as case study to develop formulations for a variety of contact types: the elastic collision between the skateboard tail and the ground, the inelastic collision between the wheels and a ground surface with discrete changes in height, and the interaction between the skateboarder's feet and the skateboard - an inelastic, frictional contact that can be applied anywhere on the skateboard's surface. With the exception of the tail-ground interaction, all formulations are unscheduled. The model we developed was able to replicate the key phases of the ollie motion, but comparison of the ground reaction force profiles to those in the literature indicates that further development is necessary for it to be a sufficiently accurate model for biomechanical analysis. The contact models behaved as expected, however, and they could easily be applied to other problems such as robotic motion planning.**

***Index Terms*—trajectory optimization, contact models, motion planning**

I. Introduction

Contacts and collisions are essential aspects of locomotion. Whether the action is something as simple as walking across a room, or as complicated as a gold-medal-winning rhythmic gymnastics routine, human movement is shaped by interactions with objects and the environment. If humanoid robots are to move in the same spaces humans are accustomed to, and complete useful tasks, their motion must be planned and controlled in a way that takes these interactions into account.

Trajectory optimization has become a valuable technique for motion planning in robotics, but modelling these contacts within a nonlinear programming problem (NLP) is challenging as they introduce discrete interruptions into the otherwise-smooth system dynamics. This creates a hybrid dynamic system [1] containing both continuous and discrete dynamics. In this paper, we develop methods of modelling a variety of contact behaviours arising in an especially dynamically-demanding activity: skateboarding. Specifically, the *ollie* manoeuvre.

Skateboarding is a sport of rapidly growing global interest. Consequently, it has been included at the 2020 Tokyo Summer Olympic Games. The ollie is a fundamental manoeuvre in skateboarding, being the simplest way to get *air* i.e. hop off the ground with the board. The high-level phases of the execution of the ollie are well-described in scientific literature [2] and skateboarder blog-styled writings [3] [4] [5]. For the purpose of this paper, the ollie will be segmented into four defined phases:

A. **Pre-"pop"**: The skateboarder pushes down on the back of the skateboard (the "tail") rotating the skateboard about its back wheel.
B. **"Pop"**: The skateboard tail strikes the ground and subsequently bounces off the ground. The skateboarder jumps into the air while simultaneously sliding his front foot up the skateboard deck.
C. **Airborne**: the skateboard and skateboarder are airborne. The skateboarder uses his feet to steady the skateboard in the air.
D. **Landing**: the skateboarder and skateboard land with the skateboarder's feet positioned above the wheel bearings.

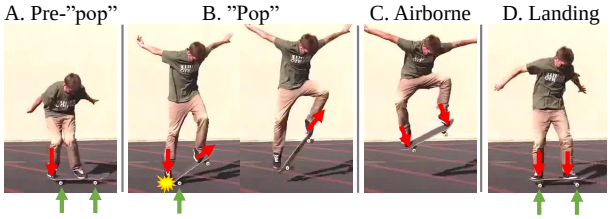

Fig. 1. The four defined phases of the ollie manoeuvre. Additionally, the ground reaction forces (GRFs), friction forces and reaction forces involved in each phase have been roughly visually represented with arrows. The picture is adapted from [6].

These phases are shown visually in Fig. 1. The ollie can be performed while stationary - the standing ollie (SO); while in motion - the rolling ollie (RO); or, up onto or down from a step - the ollie up (OU) and ollie down (OD).

Despite the continually growing popularity of skateboarding, the biomechanics of the ollie is largely unstudied and unknown. Three scientific studies have quantified the ground reaction forces (GRFs) and in-shoe forces involved in the ollie using force plates and in-shoe pressure sensors [2] [7] [8]. The results from these studies are not completely coherent, however, combining these results paints a loose picture of the peak GRFs and GRF profiles that are characteristic of the SO, RO, OD manoeuvres.

This paper will develop a trajectory optimization model of a skateboarder and skateboard that is able to replicate the ollie manoeuvre. The SO, RO and OD variations will be compared to footage of skateboarders and GRF data from the literature to

[1]The authors are with the Department of Electrical Engineering, University of Cape Town, Cape Town, 7700, South Africa (email: andnic019@myuct.ac.za; shlsta001@myuct.ac.za; a.patel@uct.ac.za

978-1-7281-4162-6/20/$31.00 ©2020 IEEE

evaluate the accuracy of the model. Besides its application to the field of sports biomechanics, this model contributes to the robotics literature as it includes novel and transferable methods for modelling the following types of contact problems:

- elastic collisions
- unscheduled contacts on surfaces with discontinuous variations in height.
- unscheduled contacts acting at any point on the surface of an object.

II. Problem Setup

The optimization problem was formulated by modeling the skateboarder and skateboard subsystems and defining the trajectory optimization problem to perform the SO, RO and OD manoeuvres.

A. Models

The modeling approach adopted for this project drew from the "templates" and "anchors" approach described by Full and Koditschek [9]: the aim of using this approach was to ensure the models encapsulated the defined key dynamics of both the skateboard and skateboarder subsystems while minimizing the complexity of the models.

For the skateboard model, a simple arrangement of rigid-links was used to represent the skateboard deck, wheel bearings and wheels. To simplify the model, shown in Fig. 2, it was assumed that the wheels and wheel bearings were of negligible mass compared to the skateboard deck. The skateboard deck has a mass of m_d, and length l_d, with a ground clearance of h_d and a wheelbase of l_w. The position and orientation of the skateboard deck is given by $({}^s x, {}^s y, {}^s \theta)$. The contact points on the deck for the back and front feet are denoted ${}^b r$ and ${}^f r$ respectively. The friction force between the wheels and the ground were neglected, leaving only the vertical GRFs, ${}^b G_y$ and ${}^f G_y$, acting on the skateboard's front and back wheels respectively.

The skateboarder model, shown in Fig. 2, was chosen as a simple biped constructed as an open kinematic chain of rigid-links. The model consisted of a torso (m_t, l_t), pelvis (m_p, l_p), a back leg with an upper (m_{b_1}, l_{b_1}) and lower (m_{b_2}, l_{b_2}) link, and a front leg also with an upper (m_{f_1}, l_{f_1}) and lower (m_{f_2}, l_{f_2}) link. The pelvis link's position and orientation is given by $({}^p x, {}^p y, {}^p \theta)$, and the torso-pelvis, back-hip and front-hip relative angles are given by ${}^t\theta$, ${}^b\theta$ and ${}^f\theta$ respectively. The links were actuated at the torso-pelvis joint by ${}^p\tau$, the back-leg-pelvis joint by ${}^b\tau$ and the front-leg-pelvis joint by ${}^f\tau$. It was decided that, since the model would be restricted to move in the coronal plane, prismatic joints [10] would be sufficient to model the propulsion or jumping motion of the human. The extension of the prismatic joints were denoted ${}^b r_k$ and ${}^f r_k$ and the joints were actuated by applied forces ${}^b F_a$ and ${}^f F_a$.

The dynamics of the each subsystem were derived independently using the Euler-Lagrange method [11] [12], with the chosen generalized coordinates:

$$\boldsymbol{q} = [{}^s x, {}^s y, {}^s \theta, {}^p x, {}^p y, {}^p \theta, {}^t \theta, {}^b \theta, {}^b r_k, {}^f \theta, {}^f r_k]^\top \tag{1}$$

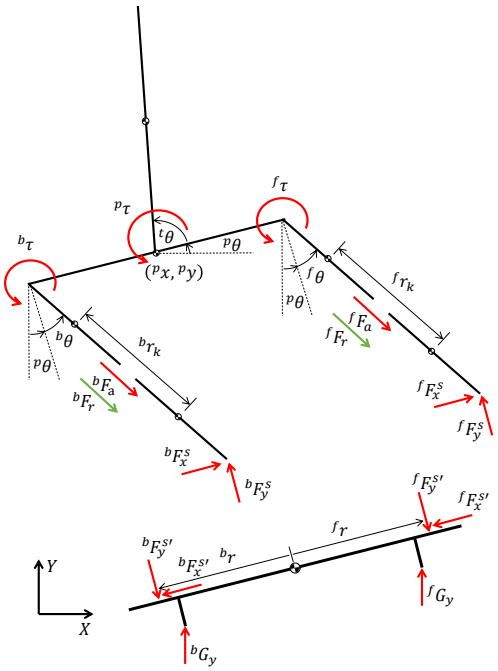

Fig. 2. Two planar models were used to model the skateboard and skateboarder. The skateboarder was modelled as an open chain of rigid-links with a torso, pelvis, and two legs modelled as prismatic joints. The skateboard was modelled using three rigid-links representing the skateboard deck, and the wheels and wheel bearings.

B. The Trajectory Optimization Problem

The problem is a boundary value problem, with the additional path constraint that the skateboard wheels should reach a height greater than 0.5m during the manoeuvre. The hybrid dynamic system was discretized with N nodes, such that $n = 1, \ldots, N$. Choosing a master time-step of $h_m = 0.01$s and considering that the ollie takes approximately 0.6s to complete [6], the number of nodes was chosen as $N = 60$. Introducing the time-step decision variable, h_n, with bounds $0.8 \leq h_n \leq 1.2$ allowed the effective time-step of the system, ${}^m h_n$, to vary by 20% of the master time-step. The effective time-step of the system can thus be defined as ${}^m h_n = h_m h_n$.

The semi-implicit Euler integration scheme was chosen for the problem as it has been shown to be useful in classical mechanics applications [10]. It was implemented as follows:

$$\boldsymbol{q}_n = \boldsymbol{q}_{n-1} + {}^m h_n \dot{\boldsymbol{q}}_n \tag{2}$$

$$\dot{\boldsymbol{q}}_n = \dot{\boldsymbol{q}}_{n-1} + {}^m h_n \ddot{\boldsymbol{q}}_{n-1} \tag{3}$$

where $\boldsymbol{q}_n$ is a column vector containing the values of the generalized coordinates at node n. Another important aspect of the optimization problem is the objective function. This was chosen to minimize the forces and torques applied by the skateboarder. The terms of the objective function were as

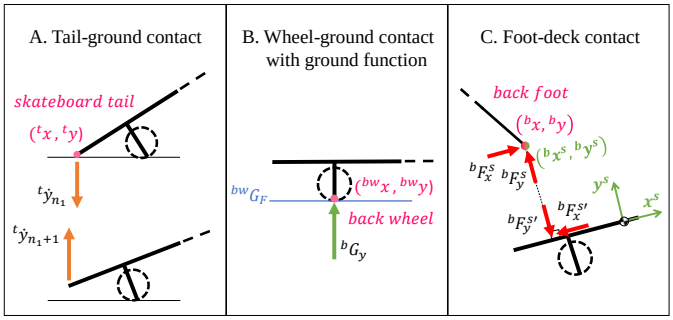

Fig. 3. The three contacts under investigation in the system and the descriptive variables used to define the tail, back wheel and back foot. Note that the position of the back foot has been described in both the inertial coordinate frame $({}^b x, {}^b y,)$ and the skateboard coordinate frame $({}^b x^s, {}^b y^s)$ [16].

follows:

$$J_F = \sum_{n=1}^{N} (({}^bF_{a,n})^2 + ({}^fF_{a,n})^2)\ {}^m h_n \tag{4}$$

$$J_\tau = \sum_{n=1}^{N} (({}^b\tau_n)^2 + ({}^f\tau_n)^2) + ({}^p\tau_n)^2)\ {}^m h_n \tag{5}$$

where J_F and J_τ are the total applied forces and torques squared.

C. Solver Specifications

The trajectory optimization problem was solved using HSL's MA86 linear solver for IPOPT [13] implemented using Python's Pyomo library [14] [15]. The solver tolerance was set to 10^{-6}.

III. Contacts

From the description of the ollie given previously, it is clear that there are elastic and inelastic collisions, as well as friction within the system. The identified contacts within the system are:

A. The tail-ground elastic collision.
B. The wheel-ground inelastic collision.
C. The foot-deck inelastic collision with friction.

These contacts are shown in Fig. 3. Two common methods implemented in literature to model hybrid dynamic systems created by elastic and inelastic collisions are the hybrid dynamics method and the contact-implicit method.

The hybrid dynamics method is a simple way of handling the discontinuous dynamics created by elastic and inelastic collisions [17] [18]. This method can be used to map a discontinuous change in state of the system at a specified guard condition. The disadvantage of using this method is that the contact sequence must be specified *a-priori*. Alternatively, the contact-implicit method described by Posa, Cantu and Tedrake [17] formulates inelastic collisions as a set of complementarity constraints in the optimization problem. This method is useful in applications involving inelastic collisions and Coulomb friction when the contact-order is largely unknown.

Combining both of these methods, the various contacts in the skateboard-skateboarder system can be formulated into the optimization problem.

A. The Tail-Ground Elastic Collision

The tail-ground collisions were modelled using the hybrid dynamics method coupled with classical mechanics in the form of the coefficient of restitution. Scheduling the collision to occur at $n = n_1$, the state mapping of the velocity of the skateboard tail is given as:

$${}^t\dot{y}_{n_1+1} = -e\,{}^t\dot{y}_{n_1} \tag{6}$$

where ${}^t\dot{y}_{n_1}$ and ${}^t\dot{y}_{n_1+1}$ are the velocities of the skateboard tail normal to the ground before and after the collision respectively, and e is the coefficient of restitution. Using this relationship, the state mapping can be expressed in terms of the generalized coordinates of the system as follows:

$${}^s\dot{y}_{n_1+1} = -e\,{}^t v_{y,n_1} + {}^s\dot{y}_{n_1} + {}^m h_n \ddot{y}_{n_1} \tag{7}$$

where ${}^s\dot{y}_{n_1}$ and ${}^s\dot{y}_{n_1+1}$ are the global y-velocities of the skateboard's centre of mass before and after the collision and $\ddot{y}_{n_1}$ is the skateboard's acceleration in the global y-direction. It was assumed that the coefficient of restitution between the skateboard tail and the ground (maple wood and concrete) was 0.6 [19].

B. The Wheel-Ground Inelastic Collision

The collision between the skateboard wheels and ground is inelastic by nature. Before the contact could be modelled, the ground function for the OU and OD manoeuvres needed to be formulated. This was achieved by utilizing complementarity relationships. Given that a step of height $y = Y_s$ occurs at position $x = X_s$, the position of the back wheel can be resolved into positive components relative to the step:

$${}^{bw}x - X_s = {}^{bw}x^{G+} - {}^{bw}x^{G-} \tag{8}$$

where ${}^{bw}x^G$ is the x-position of the back wheel relative to the step. The ground function for the back wheel, ${}^{bw}G_F$, should be bounded between the ground and step height:

$$0 \leq {}^{bw}G_F \leq Y_s \tag{9}$$

Now, the step-down ground function can be defined for the back wheel using complementarity relationships:

$$(Y_s - {}^{bw}G_{F,n})\,{}^{bw}x_n^{G-} = p_{1,n} \tag{10}$$

$${}^{bw}G_{F,n}\,{}^{bw}x_n^{G+} = p_{2,n} \tag{11}$$

where $p_{1,n}$ and $p_{2,n}$ are penalty terms included in the objective function. This can be easily extended for the step-down ground functions for the front wheel, tail and nose of the skateboard, as well as the step-up ground function.

Since the friction force between the wheels and the ground have been considered negligible, the contact-implicit method [17] can be used to formulate the complementarity constraints

needed to model the wheel-ground contact of the back wheel as follows:

$$ {}^{bw}y^G_{n+1}\ {}^bG_{y,n} = p_{3,n} \tag{12} $$

$$ {}^{bw}y^G_n,\ {}^bG_{y,n} \geq 0 \tag{13} $$

where ${}^{bw}y^G_n$ is the height of the back wheel above the ground, and ${}^bG_{y,n}$ is the GRF acting on the back wheel. It should be noted that, since the semi-implicit Euler method is being used, the GRFs are indexed one node before the position of the wheels to ensure that the GRFs can enforce the inequality constraint on ${}^{bw}y^G_n$ given in (13).

C. The Foot-Deck Inelastic Collision with Friction

The contact between the skateboarder's foot and the skateboard deck is the most complex contact in the system - it is comprised of both an inelastic collision and a friction force. Furthermore, the foot-deck contact point can vary along the length of the skateboard deck. Again, using the contact-implicit method [17], a set of complementarity constraints can be defined to formulate the foot-deck reaction force for the back foot as:

$$ {}^by^s_{n+1}\ {}^bF^{s+}_{y,n} = p_{4,n} \tag{14} $$

$$ {}^by^s_n,\ {}^bF^{s+}_{y,n} \geq 0 \tag{15} $$

where ${}^bF^{s+}_{y,n}$ is the reaction force acting on the skateboarder's back foot defined perpendicular to the skateboard. It can be seen in Fig. 3 that, by transforming the position of the foot to the skateboard reference frame, the perpendicular distance of the foot above the skateboard is given by ${}^by^s_n$. Furthermore, the foot-deck contact point on the skateboard corresponds with ${}^by^s = 0$. Therefore, the contact point on the deck can be defined as ${}^br = |\,{}^bx^s|$.

An important technique used here in place of the auxiliary variables used in [17] is to decompose a variable into a positive and negative component, with both components greater than zero. For example, in the case of the foot-deck reaction force for the back foot, this can be used as follows:

$$ {}^bF^s_{y,n} = {}^bF^{s+}_{y,n} - {}^bF^{s-}_{y,n} \tag{16} $$

$$ {}^bF^{s+}_{y,n},\ {}^bF^{s-}_{y,n} \geq 0 \tag{17} $$

where ${}^bF^{s+}_{y,n}$ and ${}^bF^{s-}_{y,n}$ are the positive and negative components of the foot-deck reaction force respectively. Similarly, this can be used for the tangential velocity of the skateboarder's back foot relative to the skateboard deck, and the friction force between the skateboarder's back foot and the skateboard, such that ${}^b\dot{x}^s_n = {}^b\dot{x}^{s+}_n - {}^b\dot{x}^{s-}_n$ and ${}^bF^s_{x,n} = {}^bF^{s+}_{x,n} - {}^bF^{s-}_{x,n}$. The foot-deck friction force can now be formulated using complementarity constraints as follows:

$$ (\mu\,{}^bF^{s+}_{y,n} - {}^bF^{s+}_{x,n} - {}^bF^{s-}_{x,n})({}^b\dot{x}^{s+}_n + {}^b\dot{x}^{s-}_n) = p_{5,n} \tag{18} $$

$$ ({}^b\dot{x}^{s+}_n)({}^bF^{s+}_{x,n}) = p_{6,n} \tag{19} $$

$$ ({}^b\dot{x}^{s-}_n)({}^bF^{s-}_{x,n}) = p_{7,n} \tag{20} $$

where μ is the coefficient of static friction between the skateboarder's foot and the skateboard deck, ${}^b\dot{x}^s_n$ is the tangential velocity of the skateboarder's back foot relative to the skateboard, and ${}^bF^s_{x,n}$ is friction force acting on the skateboarder's foot, parallel to the skateboard deck. In order to quantify the friction force, it was assumed that the underside of the skateboarder's shoe was made of rubber, and the surface of the skateboard deck was made of a sand-paper like material. Thus, it was chosen that $\mu = 0.78$ [20].

D. The Hard-Stop Joint

Since a prismatic joint was used to model the human legs, there are defined limits to the length to which the prismatic joints can linearly extend and contract. The hard-stop joint can be formulated as follows [17]:

$$ {}^bF^-_{r,n}({}^br_{k(upp)} - {}^br_{k,n+1}) = p_{8,n} \tag{21} $$

$$ {}^bF^+_{r,n}({}^br_{k,n+1} - {}^br_{k(low)}) = p_{9,n} \tag{22} $$

where ${}^bF_{r,n}$ is an internal reaction force within the prismatic joint, ${}^br_{k,n}$ is the extension of the prismatic joint, and ${}^br_{k(low)}$ and ${}^br_{k(upp)}$ are the lower and upper limits to the extension of the prismatic joint respectively.

The objective function can now be appended to include the penalty terms from the complementarity constraints:

$$ J_P = \sum_{n=1}^{N} p_{1,n} + \ldots + p_{18,n} \tag{23} $$

$$ J = J_F + J_\tau + \alpha J_P \tag{24} $$

where J_P is the penalty term. The scaling factor of $\alpha = 1000$ was used to improve the scaling of the objective function terms. The remainder of the penalty terms included in the cost function, $p_{10,n}, \ldots, p_{18,n}$, are defined for the complementarity constraints for the front wheel, front foot, front prismatic joint, and the ground function for the front wheel. The complementarity constraints were considered sufficiently minimized if J_P was below the chosen penalty violation of 10^{-6}.

IV. Results

Locally optimal solutions were obtained for the SO, RO and OD manoeuvres, with each penalty violation below the upper feasibility threshold of 10^{-6}. The motion of the biped for each simulated trajectory, shown in Fig. 4 and 5, appears to minimize energy costs and adhere to obvious physical constraints.

The simulated GRF profiles of the RO and OD and the peak GRFs are shown in Fig. 7 and 8. A three-point moving average has been applied to the GRF profiles to indicate average GRFs due to the significantly lower frequency of the simulated results to the GRF profiles from literature. The OU GRF profile from [2] was compared to the simulated RO GRF profile as the two manoeuvres are essentially identical at take-off.

V. Discussion

The simulated results were compared to the motion of the ollie observed in videos, and the existing GRF measurements from literature.

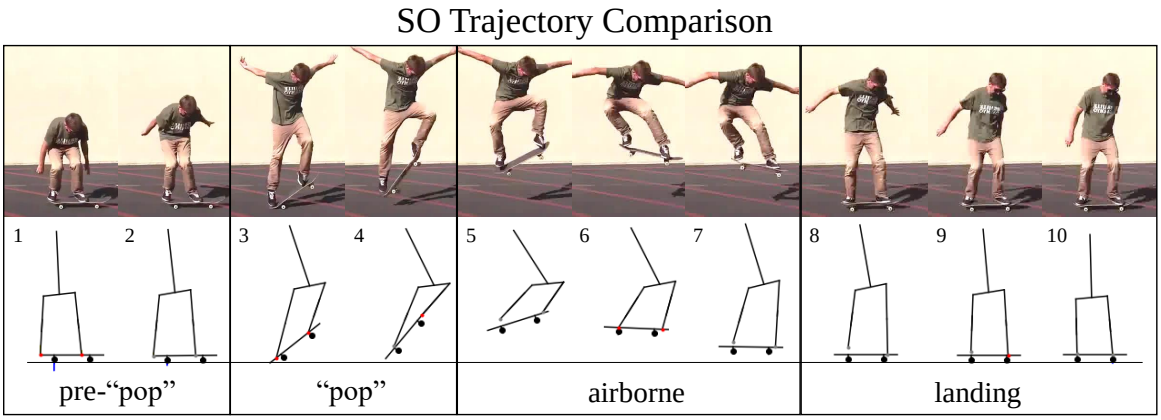

Fig. 4. A comparison of the SO simulation results to snapshots of a skateboarder performing a SO [6]. The biped model's feet are able to leave the skateboard (snaps 5, 7, 8), slide along the deck to induce a foot-deck friction force (snaps 4, 5) and apply a force onto the skateboard without mode scheduling. The skateboard "pops" off the ground (snaps 2, 3) and the wheels are able to individually interact with the ground in an unscheduled manner (snap 8).

A. Motion Analysis

The trajectory of the simulated SO, shown in Fig. 4, was compared frame by frame to snapshots of a video of a skateboarder performing a SO [6]. It can be seen that, without explicitly specifying how the biped should perform the manoeuvre, the simulated motion follows the four defined phases described previously: 1) the biped exerts a force on the skateboard tail with its back foot, rotating the skateboard about its back wheel (pre-"pop"), 2) the skateboard tail bounces off the ground while the biped slides its front foot up the skateboard deck ("pop"), 3) the skateboard and biped are airborne and the biped uses its feet to level the skateboard (airborne), and 4) the biped lands on the wheel bearings of the skateboard (landing). Additionally, since the contact-implicit method is unscheduled, the biped's feet were able to interact with skateboard deck at varying contact points and leave the deck entirely, and the skateboard wheels were able to independently make contact with the ground. These are key aspects of the ollie which the simulated system encapsulates. Discrepancies do arise in the time taken to perform the manoeuvre. The simulated system completed the ollie approximately 0.05s faster than the ollie video, however, this was deemed small enough to neglect.

Similarly, the simulated results for the RO and OD manoeuvres, shown in Fig. 5 and 6, further display clear resemblances to the real-life manoeuvres. Noticeably for the OD manoeuvre, it is clear that the biped leans back, centering its weight over its back foot, which is precisely how skateboarder's describe performing the manoeuvre [21]. An interesting aspect of the RO results, shown in Fig. 5, is that the skateboard lands on the ground before the biped lands on the skateboard ($t = 0.52$s), without any prescribed scheduling. This acts as further proof that the unscheduled contact-implicit method has been successfully implemented.

Analysing the observed trajectories of the back wheel, centre of mass, and front wheel of the skateboard shown in Fig. 6, it is again evident that the simulated and real-life trajectories

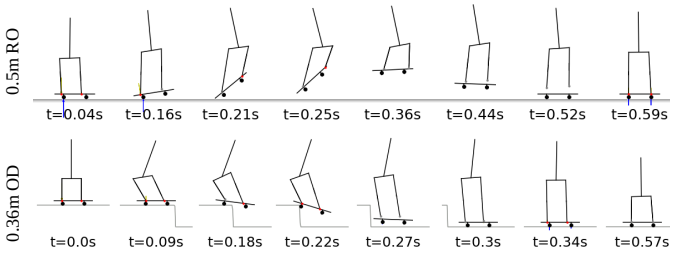

Fig. 5. The simulated results for the RO (top) and the OD (bottom) show that both trajectories resemble the expected real-life RO and OD manoeuvres. Furthermore, it can again be seen that the foot-deck and wheel-ground contacts have been implemented successfully.

are noticeably similar with slight discrepancies in the shape of the trajectories. It is worth noting that there is no perfect template for performing the ollie, particularly since the real-life manoeuvre relies on human feedback to make adjustments. Thus, it is not expected that the results will be identical.

In summary, it is evident that the trajectory of the simulated system performing the ollie manoeuvres replicates both the defined phases of the SO, and, to a large extent, the visual real-life motion of the SO, RO and OD manoeuvres.

B. GRF Analysis

The next metric for comparison of the simulated results is the peak GRF results and the GRF profiles. This is particularly important to assess how appropriate this model is for biomechanics studies. The RO and OD GRF profiles, shown in Fig. 7, are significantly different in magnitude and shape. After applying the three-point moving average function, there is a greater resemblance in the profiles, particularly in the positioning of the local and global mimima, however, the resemblance is still minimal. Looking at the comparison of the peak GRF results shown in Fig. 8, it is evident that only the results of the OD at take-off and the SO at landing fall within one standard deviation of the results obtained in literature [2]

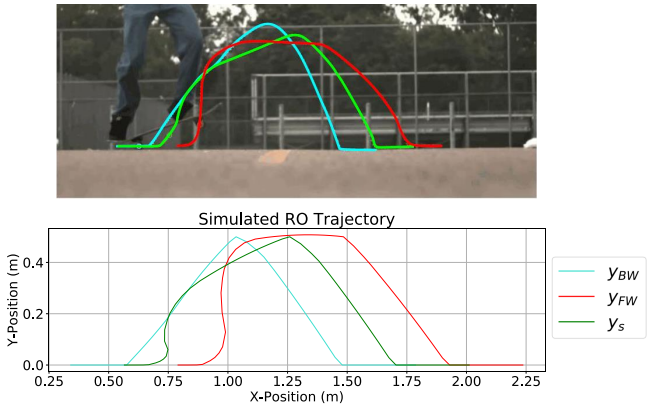

Fig. 6. A comparison of the RO trajectory provided by Bhatia [5] and the simulated RO trajectory of the back and front wheels, and the skateboard's centre of mass.

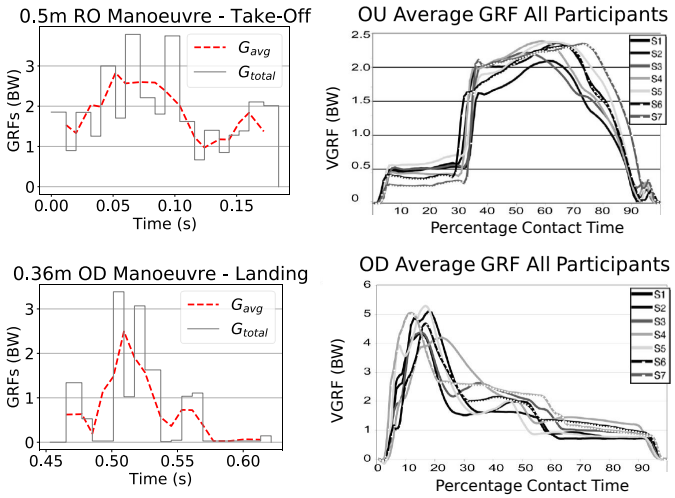

Fig. 7. The GRF profiles for the RO at take-off compared to the OU at take-off from [2] (top) and the OD at landing compared to the OD at landing from [2] (bottom).

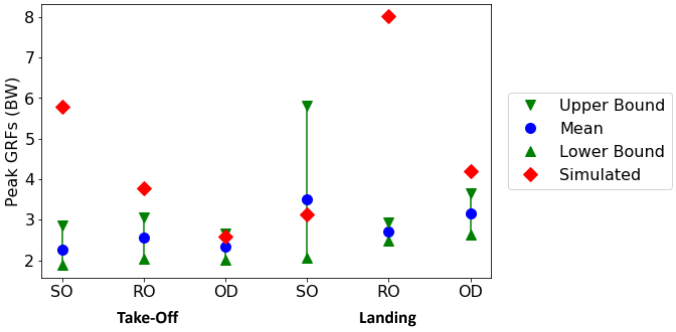

Fig. 8. The simulated peak GRFs for the SO, RO and OD at take-off and landing compared to the measured results from literature [2] [7]. Only the simulated OD at take-off and SO at landing fall within the one standard deviation bounds given in literature.

[7]. The simulated SO take-off and RO landing peak GRFs differ most significantly, at approximately 2.8 BW and 4.9 BW respectively. These differences are too significant to conclude that the simulated GRF results replicate the measured results from literature.

Considering the simplicity of the chosen integration scheme and the low number of nodes chosen for the trajectory optimization problem, these results are far more similar to the GRFs recorded in literature than expected. Additionally, the discrepancies between the simulated and real-life measured GRF results suggest that there may have been oversight regarding the assumption made in modelling the system. It was identified that modeling the human as a biped, with legs modelled as rigid links connected by a spring-damper-less prismatic joint, may have been the major contributor to the discrepancies between the GRF results obtained. Thus, it is possible that the biped model used to model the skateboarder lacked the required complexity to encapsulate the key dynamics of the skateboarder.

VI. Conclusion

Through the case study of the skateboarding ollie manoeuvre, we have demonstrated methods for which the trajectory optimization problem can be formulated for hybrid dynamic systems with elastic and inelastic multi-body collisions. This was achieved by using the hybrid dynamic method in conjunction with the contact-implicit method which combined both scheduled and unscheduled motion planning.

Additionally, it was shown that the simple biped and skateboard models were of the required complexity to replicate the ollie motion. While the individual contact models performed as desired and are potentially transferable to other applications, due to the discrepancies in the simulated and real-life GRFs, the overall system needs further development in order to be useful in biomechanics applications.

Further Resources

Trajectory optimization is a daunting topic to tackle whether you are an undergraduate or a professor. For more information on trajectory optimization, see Matthew Kelly's blog [22]. Also, Stacey Shield has provided simple Jupyter Notebooks which are a great introduction to the theory used in this study [23].

References

[1] R. Goebel, R. G. Sanfelice, and A. R. Teel, "Hybrid dynamical systems," *IEEE Control Systems Magazine*, vol. 29, no. 2, pp. 28–93, 2009.

[2] E. C. Frederick, J. J. Determan, S. N. Whittlesey, and J. Hamill, "Biomechanics of skateboarding: Kinetics of the ollie," *Journal of applied biomechanics*, vol. 22, no. 1, pp. 33–40, 2006.

[3] "Jumping: the ollie." [Online]. Available: https://www.exploratorium.edu/skateboarding/trick02.html

[4] "Learn how to ollie with skateboard trick tips." [Online]. Available: http://www.skateboard-trick-tips.com/tricktips/ollie.html

[5] A. Bhatia, "The physics of doing an ollie on a skateboard, or, the science of why i can't skate," 2014. [Online]. Available: https://www.wired.com/2014/10/skateboard-physics-empzeal/

[6] "5 steps to better ollies," 2015. [Online]. Available: https://www.youtube.com/watch?v=OrOZxOTIv-g

[7] A. Leuchanka, J. Ewen, and B. Cooper, "Bipedal in-shoe kinetics of skateboarding–the ollie," *Footwear Science*, vol. 9, no. sup1, pp. S122–S124, 2017.

[8] J. Determan, E. Frederick, J. Cox, and M. Nevitt, "Kinetics of the skateboarding kick flip," *Journal of Biomechanics*, vol. 39, no. 1, p. S188, 2006.

[9] R. J. Full and D. E. Koditschek, "Templates and anchors: neuromechanical hypotheses of legged locomotion on land," *Journal of experimental biology*, vol. 202, no. 23, pp. 3325–3332, 1999.

[10] W. Xi and C. D. Remy, "Optimal gaits and motions for legged robots," in *2014 IEEE/RSJ International Conference on Intelligent Robots and Systems*. IEEE, 2014, pp. 3259–3265.

[11] R. M. Murray, *A mathematical introduction to robotic manipulation*. CRC press, 2017.

[12] D. T. Greenwood, *Advanced dynamics*. Cambridge University Press, 2006.

[13] HSL, "A collection of fortran codes for large scale scientific computation." [Online]. Available: http://www.hsl.rl.ac.uk/

[14] W. E. Hart, C. D. Laird, J.-P. Watson, D. L. Woodruff, G. A. Hackebeil, B. L. Nicholson, and J. D. Siirola, *Pyomo–optimization modeling in python*, 2nd ed. Springer Science & Business Media, 2017, vol. 67.

[15] W. E. Hart, J.-P. Watson, and D. L. Woodruff, "Pyomo: modeling and solving mathematical programs in python," *Mathematical Programming Computation*, vol. 3, no. 3, pp. 219–260, 2011.

[16] J. Diebel, "Representing attitude: Euler angles, unit quaternions, and rotation vectors," *Matrix*, vol. 58, no. 15-16, pp. 1–35, 2006.

[17] M. Posa, C. Cantu, and R. Tedrake, "A direct method for trajectory optimization of rigid bodies through contact," *The International Journal of Robotics Research*, vol. 33, no. 1, pp. 69–81, 2014.

[18] C. Hubicki, M. Jones, M. Daley, and J. Hurst, "Do limit cycles matter in the long run? stable orbits and sliding-mass dynamics emerge in task-optimal locomotion," in *2015 IEEE International Conference on Robotics and Automation (ICRA)*. IEEE, 2015, pp. 5113–5120.

[19] J. Bennet and R. Meepagala, "Coefficients of restitution," 2006. [Online]. Available: https://hypertextbook.com/facts/2006/restitution.shtml/

[20] E. H. Bani-Hani, J. Lopez, and G. Mohanan, "Data on the coefficient of static friction between surfaces coated with different sizes of rubber granules produced from used tires," *Data in brief*, vol. 22, pp. 940–945, 2019.

[21] "Teaching zexy zek to ollie!" 2018. [Online]. Available: https://www.youtube.com/watch?v=6Y1got6iF_A

[22] M. Kelly, "Trajectory optimization." [Online]. Available: http://www.matthewpeterkelly.com/tutorials/trajectoryOptimization/index.html

[23] S. Shield, "Pyomo tutorials," 2019. [Online]. Available: https://github.com/UCTMechatronics/pyomo_tutorials